Research Article

Surface photosensitization of ZnO by ZnS to enhance the photodegradation efficiency for organic pollutants

Sunaina[1,2] · Sapna Devi[1] · S. T. Nishanthi[1,4] · S. K. Mehta[2] · A. K. Ganguli[1,3] · Menaka Jha[1]

Abstract

It is challenging to develop a material which has low cost, high activity, good stability and recyclability under light exposure. Apart from these properties, the photocatalyst should also have good visible region absorbance and low electron-hole pair recombination rate. Keeping all this in view, we have designed a simple scalable synthesis of ZnO–ZnS heterostructures for the photocatalytic treatment of industrial waste (*p*-nitrophenol and methyl orange). The ZnO–ZnS heterostructures are synthesized via a solvent-free route by thermal annealing of solid-state mixture of ZnO and thiourea (a sulphur source) which results in ZnO–ZnS core shell kind of heterostructure formation. The interface formation between the ZnO–ZnS heterostructure favored the band-gap reduction in comparison to the bare ZnO and ZnS nanoparticles. Further, these ZnO–ZnS heterostructures were utilized as a photocatalyst for the degradation of toxic phenolic molecules (*p*-nitrophenol) and harmful organic dyes (methyl orange) present in the water under the light exposure (> 390 nm).

1 Introduction

Designing the metal oxide based photocatalyst for environmental pollution control has gained a lot of research interest worldwide [1–3]. Between all the various metal oxides, TiO_2, ZnO, SnO_2 based photocatalysts are some of the most studied systems [4–6]. ZnO is one of the best candidates which has great response as a photocatalyst. However, the commercial usage of ZnO is limited because low quantum efficiency and instability in wide pH range due to photo-corrosion. This limitation has led to research oriented towards improving the ZnO properties by forming heterostructure or doping with other materials [7–9].

In the case of heterostructures, core-shell structures have an advantage where the shell can be a physical barrier between the optically active core and the surrounding medium. It can also modify the charge, stability, functionality, reactivity, and dispersive ability of core material [10–14]. Core shell heterostructures also have better electrical, catalytic, optical, and magnetic properties in comparison to their bare counter parts [15–17]. Generally, the core-shell heterostructures have intermediate properties between the core and shell materials [18–20]. Khanchandani et al. have synthesized ZnO–CdS, ZnO–Ag_2S and ZnO–In_2S_3 core-shell heterostructures. They have functionalized the ZnO surface by using the citric acid and

---

✉ A. K. Ganguli, menaka@inst.ac.in; ✉ Menaka Jha, menaka@inst.ac.in | [1]Institute of Nano Science and Technology, Mohali 140306, India. [2]Department of Chemistry, Panjab University, Chandigarh 160014, India. [3]Department of Chemistry, Indian Institute of Technology, New Delhi 110016, India. [4]ECPS Division, CSIR-Central Electrochemical Research Institute, Karaikudi, Tamil Nadu 630003, India.

then formed CdS or Ag_2S or In_2S_3 shell over a ZnO core by chemical route. These core/shell nanostructures show superior photocatalytic behavior for the degradation of dyes under light illumination [21–23]. Subash et al. prepared the Ag_2S–ZnO composite via a two-step process. They first precipitated the zinc oxalate and Ag_2S and then calcined the mixture at 400 °C for 12 h to obtain Ag_2S–ZnO composite. The photodegradation of Acid Black 1 was performed by using Ag_2S–ZnO composite under solar light. The composite was more capable for mineralizing the Acid Black 1 in comparison to synthesized ZnO, bulk ZnO, TiO_2–P25 and TiO_2 (Merck) [24]. Shi et al. have synthesized the ZnO–PbS/GO photocatalyst for hydrogen evolution from water. The multiple exciton formation in ZnO–PbS/GO is responsible for the remarkable enhanced photoactivity of H_2 evolution reaction [25]. The above researches show that the formation of core-shell heterostructures by incorporating the metal sulfide shell on to the ZnO core enhances its absorption in the visible range which further improves the photocatalytic reaction efficiency by increasing the stability of electron-hole pairs. Zinc sulphide (ZnS) is a wide band gap (3.7 eV) semiconductor material which is nontoxic and water insoluble [26, 27]. It can be used as a coating material for ZnO nanorods because it has shown its application in electroluminescent devices, sensors and lasers [28–31]. ZnO–ZnS based heterostructures have shown improved physicochemical properties in different applications [32–36]. Hence, a considerable efforts have been made to synthesize ZnO–ZnS based heterostructures [37–42]. Lin et al. have made an efficient ZnO–ZnS photocatalyst using template-assisted method. The photo-activity of ZnO–ZnS photocatalyst was analyzed by using degradation of rhodamine B. The surface coupling between the two semiconductors proposes their higher photon absorption efficiency and an enhanced exciton separation, which lead to a significant improvement in the photocatalytic efficacy in comparison with bare ZnO [43]. Lonkar et al. have prepared the ZnS–ZnO/graphene based nano-photocatalysts. The ZnO and ZnS nanoparticles are uniformly distributed over the graphene matrix in the synthesized nanohybrids. The synergic effect in ZnS–ZnO/graphene decreased the band gap in the composite system. They checked the photocatalytic efficiency of ZnS–ZnO/graphene nano–photocatalysts by a test photo-reaction with organic azo dyes and toxic phenol molecules from waste water which have harmful impact on the environment [44]. Based on the above literature survey, it appears that the heterojunction formation between the ZnO and ZnS will generate superior hybrid material having lower photoexcitation energy than the bare counter parts [32–44]. The reason behind this is ZnO–ZnS heterostructures induces a built-in electric field which improve the interfacial charge transfer and deliver remarkable photoactivity [32–44]. Theoretically, type II band alignment formed between ZnO and ZnS results in the better photocatalytic activity in the heterostructure. Therefore, ZnO–ZnS heterostructure represents a fascinating candidate for photocatalysis. Here, we have attempted to a simplistic one-pot bulk approach for synthesize of ZnO–ZnS core-shell heterostructures through solid state solvent free route. Earlier, the typical methods which are used for the synthesis of ZnO–ZnS heterostructures consist of solvothermal route, sol–gel process, microwave route, ion replacement etc. The large solvent usage and the complex synthetic procedure limited their usage for large scale productions. Here, we did the sulphurization of ZnO nanorods by utilizing the thiourea as sulphur source. The amount of ZnO and ZnS in the heterostructures can be controlled by varying the amount of thiourea used in the reaction. These fabricated heterostructures were thoroughly characterized using PXRD, TEM, EDX, UV-Vis spectroscopy, PL, EPR, EIS and XPS studies. Further, the as synthesized ZnO–ZnS heterostructures were utilized for removal of industrial waste water containing the organic pollutants (p-nitrophenol and methyl orange).

2 Materials and methods

2.1 Material used

For the preparation of ZnO, ZnS and ZnO–ZnS heterostructures, zinc acetate dihydrate (Sigma-Aldrich, purity 98%) and thiourea (Merck, purity 99%) were utilized. p-nitrophenol (PNP, Fluka, > 98%) and methyl orange (MO, Sigma-Aldrich, 98%) were used as representative chemicals for industrial waste effluent treatment. Benzoquinone (Sigma-Aldrich, purity 98%), Ammonium oxalate (Merck, purity 99%) and isopropanol (Merck, purity 99%) were used as trapping agents to identify the active species responsible for the photocatalytic activity of ZnO–ZnS heterostructures.

2.2 Synthesis procedure

ZnO nanorods were synthesized by solid state route. Briefly, zinc acetate was thermally decomposed in a muffle furnace for 12 h at 300 °C with a heating rate of 40 °C/h. Pure ZnS was synthesized by putting equimolar zinc acetate and thiourea in furnace under same condition. The ZnO–ZnS heterostructures were synthesized by taking different molar ratio of ZnO nanorods and thiourea in a mortar pestle and grounded to fine powder (Table 1). Then the resulting solid mixture was calcined in a muffle furnace under similar condition. The obtained product was washed with water and ethanol to remove unreacted thiourea.

Table 1 Parameters for the synthesis of ZnO–ZnS heterostructure formation

Zinc precursor	Sulphur source	Molar ratio	Phase observed from PXRD	Sample code
Zinc acetate	–	1:0	ZnO	Z1
Zinc acetate	Thiourea	1:1	ZnS	Z2
ZnO	Thiourea	1:1	ZnO–ZnS	Z3
ZnO	Thiourea	1:2	ZnO–ZnS	Z4
ZnO	Thiourea	1:4	ZnO–ZnS	Z5

2.3 Characterization

The characterization of phase formed, their purity and crystal structure of the products were carried out on a powder X-ray diffractometer (Bruker D8 Advance diffractometer) having Ni filtered Cu Kα radiation with wavelength 1.54060 Å in the range of 10°–80° with a scan rate 0.02°. The morphology studies of the samples were done on a transmission electron microscope (JEOL, JEM-2100) operated at 200 kV. The band gap of the samples was calculated using DRS studies on a UV-vis spectrophotometer (Shimadzu, UV-2600). The band gaps (E_g) were evaluated using following Tauc equation –

$$(\alpha h\nu)^n = k(h\nu - E_g) \qquad (1)$$

where h is Planck's constant, ν is the frequency of photon, α is the absorption coefficient, k is a constant and n is 2 or ½ depending on direct transition or indirect transition respectively.

The evaluation of photocatalytic activity of ZnO–ZnS heterostructures for p-nitrophenol and methyl orange dye has been done under a 300 W Xenon lamp (Newport) with 390 nm filter. The absorbance spectra were measured using an UV-Vis spectrophotometer (Shimadzu 2600, Japan). The absorbance spectra as measured after every 10 min under light illumination. The details of photocatalytic procedure are given in supplementary information. The photocatalytic measurements for degradation of MO dye using the ZnO–ZnS heterostructures were also performed under the standard conditions by using commercial AM 1.5G solar simulators. Electrochemical studies for measuring the EIS and transient photoresponse of the heterostructure performed in a three-electrode PGSTAT-30 (Autolab) electrochemical work station. EPR studies were performed on Bruker EMX Plus instrument. X-ray photoelectron spectroscopy (XPS) studies were carried out with an ESCALAB 250Xi (Thermo Scientific) operating with an Al Kα source (1486.6 eV) under an ultrahigh vacuum of 3.5×10^{-7} Pa.

3 Results and discussion

In the present study, an attempt has been made to design an efficient photocatalyst for industrial pollutant degradation. The work has been done in two stages and in the first stage, ZnO–ZnS heterostructures were synthesized via solid state (solvent free) route by changing the molar ratio of ZnO and thiourea. Second stage deals with the photocatalytic studies of the synthesized heterostructures for removal of industrial pollutants (here methyl orange and p-nitrophenol) and their detailed mechanistic studies. The phase and crystal structure of all synthesized samples was determined by PXRD. Figure S1a shows the PXRD pattern of the product obtained after the thermal decomposition of zinc acetate at 300 °C for 12 h. After the thermal treatment, the observed PXRD pattern of Z1 indicates the formation of hexagonal ZnO having space group P6₃mc (JCPDS-01-071-6424). Similarly, the product obtained from the thermal decomposition of mixture of equimolar ratio of zinc acetate and thiourea (Z2) has been analyzed by PXRD (Fig. S1b). All the reflection planes could be indexed using the hexagonal unit cell of ZnS to the P3m1 space group (JCPDS-01-072-9267). As discussed earlier, here we aim to synthesis ZnO–ZnS heterostructure and from above phase analysis; we found that utilization of zinc acetate leads to the formation of either ZnO or ZnS. Hence, to make the heterostructures, we have first attempted to synthesize the ZnO nanorods by calcining the zinc acetate at slow heating rate. The as obtained ZnO was further sulphurized using thiourea. For this purpose, ZnO was ground with thiourea in different molar ratio and heated at 300 °C for 12 h (Table 1 and experimental section). PXRD pattern of Z3, Z4 and Z5 are given in Fig. 1. All the diffraction peaks in PXRD pattern was well matched with ZnO (JCPDS no.01-071-6424) and ZnS (JCPDS no. 01-072-9267). As we increase the quantity of thiourea, the percentage of ZnS increased (Fig. 1b–d). Additionally, there are no extra peaks in PXRD pattern which confirms the formation of ZnO–ZnS heterostructures. From the powder x-ray
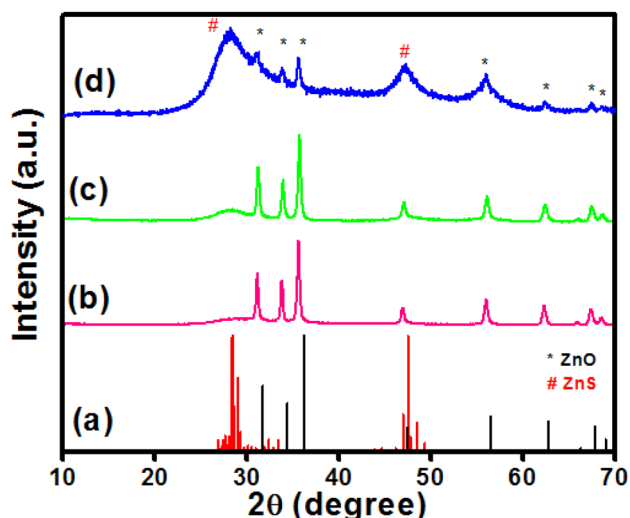
Fig. 1 Powder X-ray diffraction patterns of **a** standard peaks for ZnO and ZnS, **b** Z3, **c** Z4 and **d** Z5

diffraction study, it appears that when ZnO were thermally treated with thiourea, there is partial conversion of ZnO into ZnS by interaction of zinc oxide surface with thiourea at 300 °C [45]. The size and morphological characteristics of synthesized samples were analyzed under transmission electron microscopy (TEM). Figure 2 displays the TEM micrographs of the as-synthesized Z1, Z2, Z3, Z4 and Z5. In the case of Z1 (bare ZnO), the nanorods of size 25 nm × 390 nm with an aspect ratio of 14 were observed. As discussed earlier, zinc acetate and thiourea were heated

together and ZnS was formed. TEM micrograph indicates the formation of 10–15 nm particles. To make the heterostructures, ZnO nanorods were heated with thiourea. These heterostructures have core-shell type of structure with inner core of ZnO and ZnS shell as shown in Fig. 2c,e. The TEM micrographs of the ZnO–ZnS heterostructures show the formation of nanorods of size 65 nm × 375 nm for Z3 with shell thickness 15 nm, 75 nm × 335 nm with shell thickness 20 nm, 90 nm × 300 nm for Z5 with shell thickness 23 nm. In Fig. 2, TEM micrographs of the ZnO–ZnS heterostructure shows that ZnS nanoparticles are attached on to the surface of ZnO nanorods uniformly which enables effective interfacial electron transfer, thus, an increased photocatalytic activity is expected in heterostructures. The results of line EDX mapping (Fig. 3) show that there is co-existence of Zn, O and S elements in ZnO–ZnS core/shell heterostructures. Fig 3 demonstrates the results of TEM line-EDX mapping acquired by positioning the electron beam across the ZnO–ZnS nanorods. Positioning the electron beam across the ZnO–ZnS heterostructure resulted in significantly intense homogeneous signals of Zn and S in the shell and weaker signals of O beam across the ZnO–ZnS nanorods respectively. This analysis confirms the composition of ZnO–ZnS heterostructures have ZnO as core and ZnS as the shell material. Thus, the EDX analysis, gives the clear evidence of the formation of a core/shell heterostructure [46]. The insights of surface properties and components in the synthesized samples were obtained by XPS studies. The plots for all the samples are shown in Fig. 4 and S2. The surface O 1 s peak
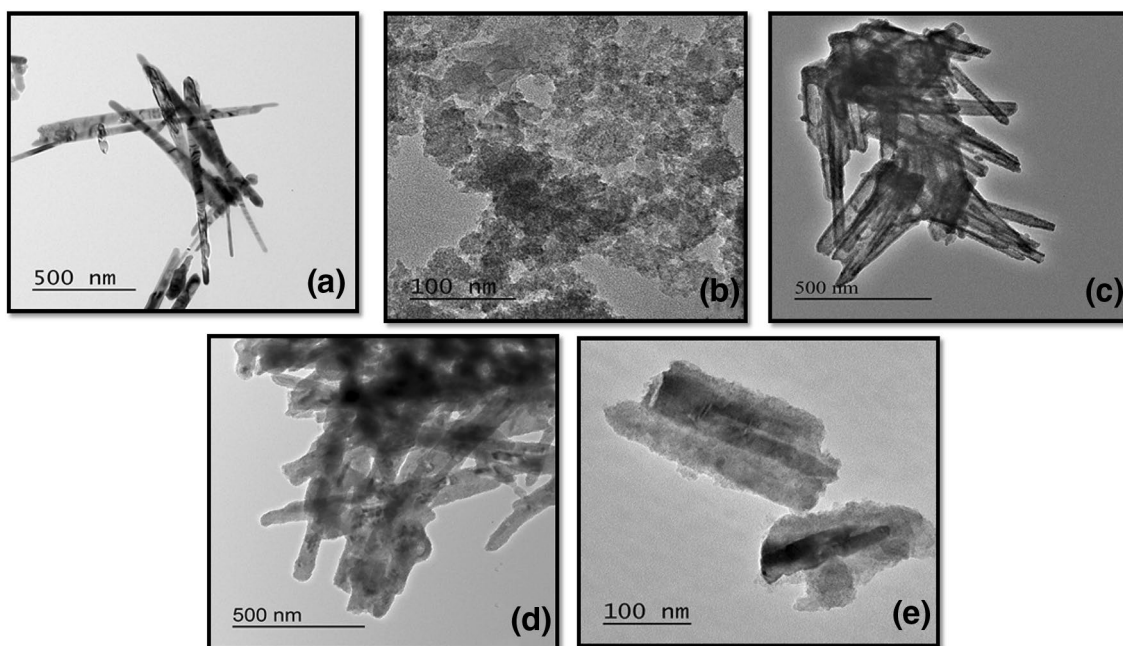

Fig. 2 TEM micrographs for the **a** Z1, **b** Z2, **c** Z3, **d** Z4 and **e** Z5
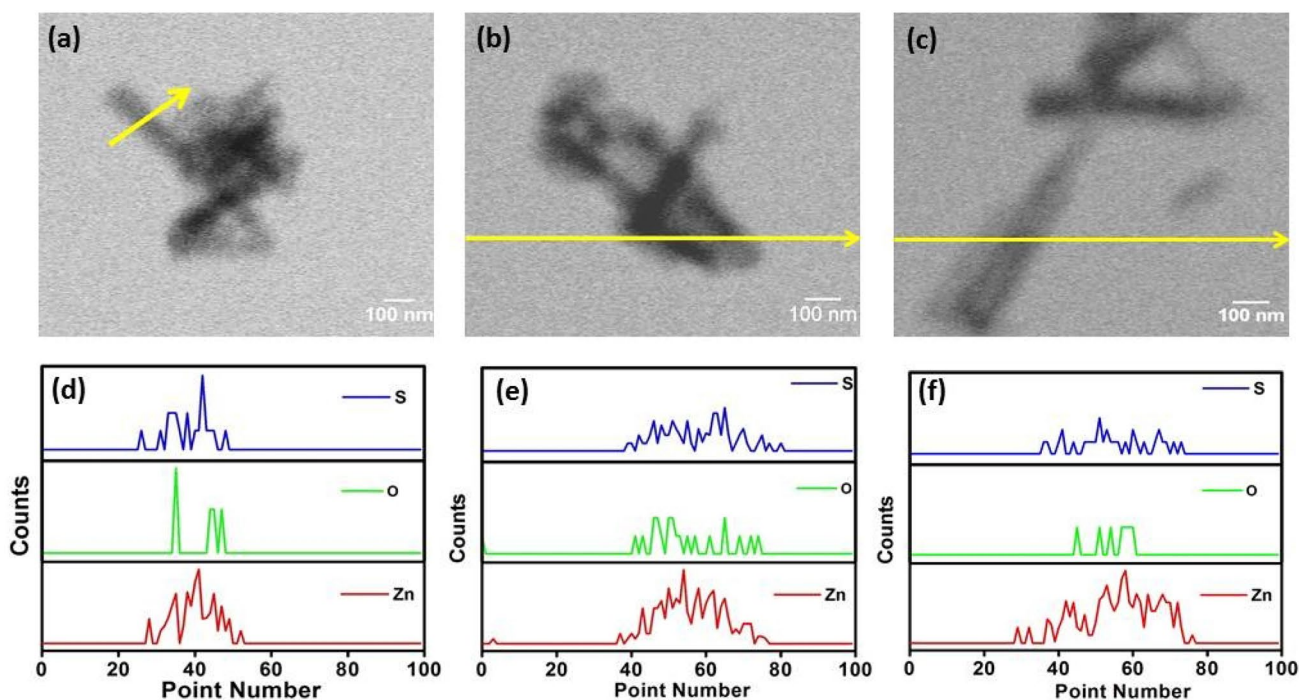
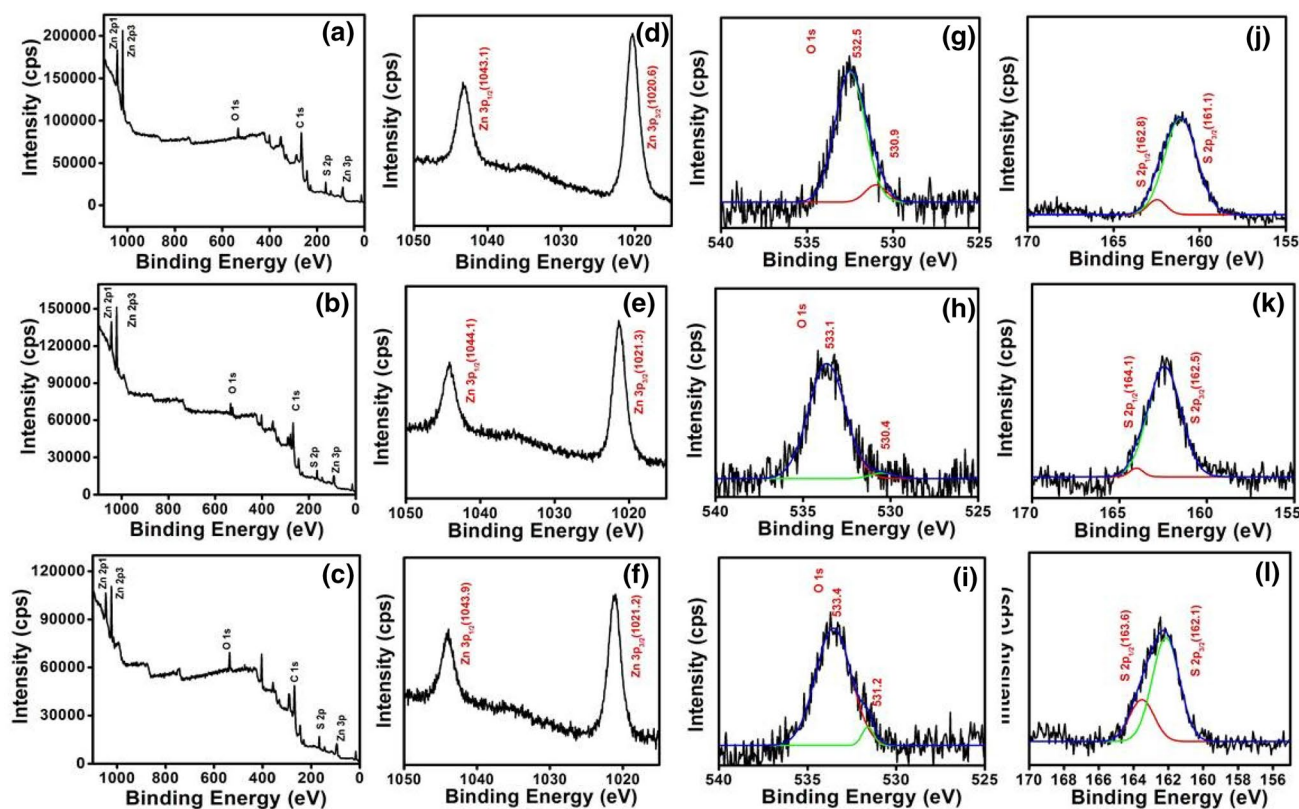**Fig. 3** STEM micrographs and their corresponding line mapping **a, d** Z3, **b, e** Z4 and **c, f** Z5

Fig. 4 a-c Fully scanned XPS spectra, high-resolution XPS spectrum of **d-f** Zn 2p, **g-i** O 1 s and **j-l** S 2p of Z3, Z4 and Z5 heterostructures respectively

contained contributions from different chemical species in relative to the processing conditions. The $Zn2p_{3/2}$ and $Zn2p_{1/2}$ peaks at ~ 1020 and ~ 1043 eV, respectively, are shown in Fig. 4d-f. Besides the presence of lattice oxygen located at 530.0 eV which is an indication of ZnO formation, a second band centered at ~ 532 eV is assigned to the chemisorbed oxygen caused by surface hydroxyl groups. In the S2p XPS spectra (Fig. 4g–i), the $S2p_{3/2}$ and $S2p_{1/2}$ peaks centered at ~ 161 and ~ 163 eV, respectively, are related to Zn−S bonding, indicating that ZnS has been successfully synthesized. Compared with the pure ZnO, O 1 s peak at around 531.9 eV was detected and shifted after the deposition of ZnS nanoparticles, and the peak area at 530.0 eV of lattice oxygen decreased sharply (Fig. 4 and S2), which shows that almost no ZnO crystal exists in the ZnS shell layer [47–49]. The optical band gap determined for ZnO, ZnS and ZnO–ZnS heterostructures by using UV/vis diffuse reflectance spectroscopy (DRS) and the values calculated for Z1, Z2, Z3, Z4 and Z5 were found to be 3.3, 3.6, 3.1, 3.1 and 3.1 eV, respectively (Fig. S3). This shift in the absorption energy can be ascribed to the sensitization of ZnS. When the ZnO nanorods are covered with the ZnS shell, there is Type II kind of heterojunction formation. In a Type II heterostructure, the bandgap effectively reduced in comparison to the core and shell material. Decrease in bandgap will make the heterostructure to absorb the lower energy light to generate the charge carriers and also favors the fast charge transport across the heterojunction. This observation shows that ZnO–ZnS heterostructures can show better photocatalytic activity. BET adsorption–desorption isotherms of ZnO, ZnS and ZnS–ZnO heterostructures are shown in Fig. S3a. BET surface area of the ZnS–ZnO heterostructures are larger than those of bare ZnO, which indicates that the resulting heterostructures can provide a larger interface to enhance the contact between the dye and the active catalyst and facilitate photocatalytic reaction. The BJH pore size distribution curves of all the samples are shown in Fig. S3b. The mesoporosity in the resulting heterostructures was further confirmed from the pore size distribution peaks that are centered on a 2 nm and a broad peak around 6–8 nm. The measured BET surface areas and average pore radius for ZnO, ZnS and ZnS–ZnO heterostructures are presented in Table S1. After heterojunction formation, the surface areas tend to increase due to surface decoration of ZnO nanorods with ZnS nanoparticles, this further evidence the *in-situ* formation of nanostructured heterostructures [50]. Photocatalytic behavior of the synthesized ZnO, ZnS and ZnO–ZnS heterostructures is evaluated in comparison to bare ZnO and ZnS through photo-degradation studies of p-nitrophenol (PNP) and Methyl Orange (MO) dye under light exposure (> 390 nm). Before illuminating the light over catalyst containing PNP or MO solution, the solution is

kept in dark to acquire the adsorption–desorption equilibrium. The UV-vis absorption spectra for the reduction of PNP in aqueous medium using $NaBH_4$ with addition of the catalyst (1 mg/mL) are shown in Fig. 5. The pure PNP shows a λ_{max} at 317 nm in aqueous medium and when the $NaBH_4$ is added to it, a red shift occurs from 317 to 403 nm due to the formation of p-nitrophenolate ions. The yellow color of the PNP solution thus disappeared as the photocatalytic reaction proceeds. In the case of bare Z1 or Z2, there was insignificant photodegradation of PNP (Fig. 5a, b), whereas, in the case of Z3, Z4 and Z5 heterostructures, there is an increased photodegradation of PNP under light illumination (Fig. 5c, d). In case of Z3, Z4 and Z5, there is appearance of a new peak ~ 297 nm which corresponds to formation of p-aminophenol [51]. Figure 5f shows that in the absence of any photocatalyst, there is no degradation of PNP under light irradiation which indicates the photocatalytic nature of ZnO–ZnS heterostructures. The comparison and the kinetics of photodegradation of PNP in the presence of heterostructures are shown in Fig. 6 and Table 2. The reaction rates of Z1, Z2, Z3, Z4 and Z5 were 0.012, 0.002, 0.037, 0.030 and 0.024 min^{-1} respectively. The Z3 sample is showing the best results for PNP photodegradation with an efficiency of ~ 90%. Further, the photodegradation of MO dye has been done and mechanistic studies have been explored. Fig 7 shows a typical UV-vis spectrum of MO by Z1, Z2, Z3, Z4 and Z5 for 60 min. Methyl orangedye has an azo group which acts as chromophorewhich gives its characteristic absorptionmaximum at 464 nm. The illumination of light over MO in the presence of photocatalyst causes the breakage of this azo bond hence the intensity is decreased at 464 nm with time. Fig 8 depicts the comparison of photo-catalytic activities of ZnO–ZnS heterostructures with respect to bare ZnO and ZnS under light exposure. The efficiency of bare ZnO or ZnS is comparatively lower than those of heterostructures (Fig. 8a). Z3 is showing the maximum efficiency ~ 97% for MO degradation. The rate kinetics for the photodegradation of MO by all the samples follows the pseudo first order reaction (Fig. 8b and Table 3). The reaction rates were for pure Z1, Z2, Z3, Z4 and Z5 are 0.006, 0.001, 0.049, 0.039 and 0.014 min^{-1}, respectively. Fig 8c shows the reusability of Z3 for photocatalytic degradation of MO up to three cycles. The decrease in the photocatalytic efficiency of Z3 after the 3rd cycle is from 97 to 89%. Table 4 shows the comparison of the prepared ZnO–ZnS photocatalysts with the literature. The photocatalytic measurements for degradation of MO dye using the ZnO–ZnS heterostructures were also performed under the standard conditions by using commercial AM 1.5G solar simulators (Fig. S5). The results obtained using commercial AM 1.5G solar simulators were corroborated with the results obtained from Xenon lamp experiments (Fig. S6 and Table S2). The
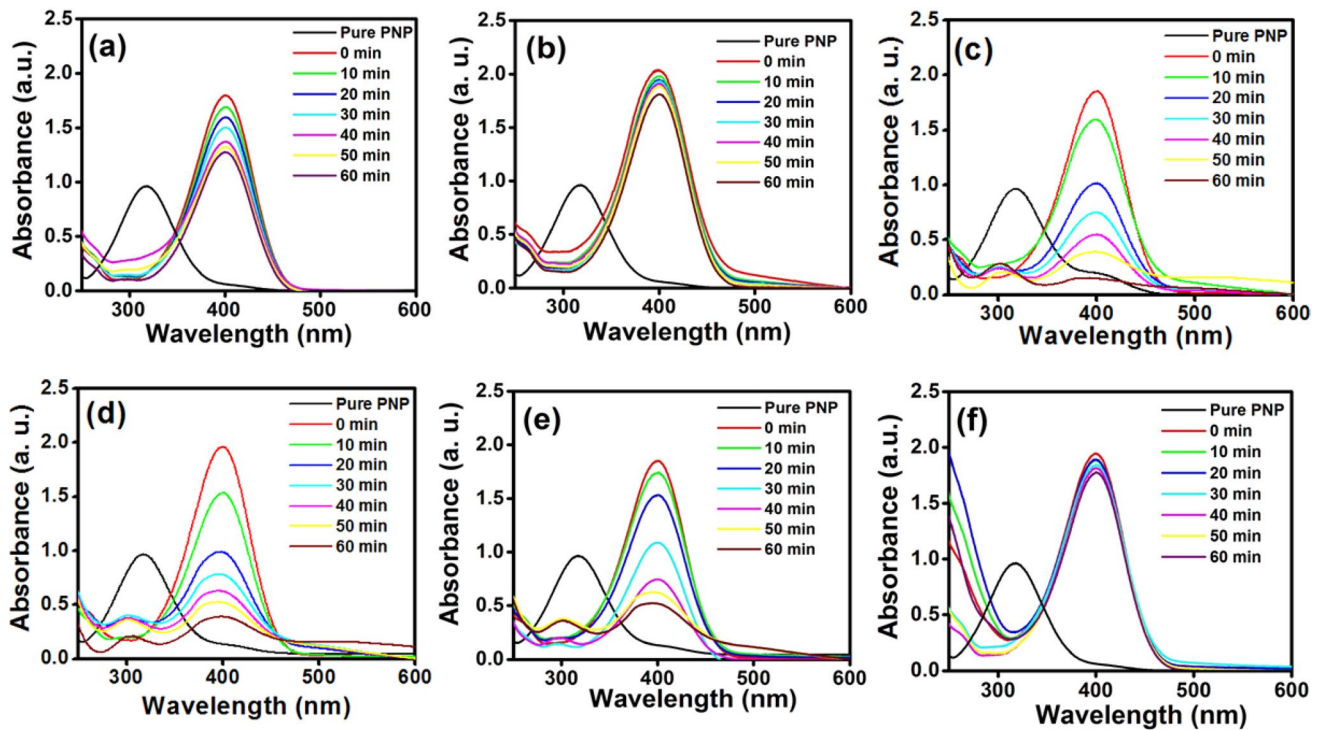
Fig. 5 Photo-degradation study of p-nitrophenol under light illumination containing photocatalyst **a** Z1, **b** Z2, **c** Z3, **d** Z4, **e** Z5 and **f** no catalyst

Fig. 6 a Comparison and **b** kinetics of Photo-degradation of *p*–nitrophenol under light illumination containing different photocatalyst
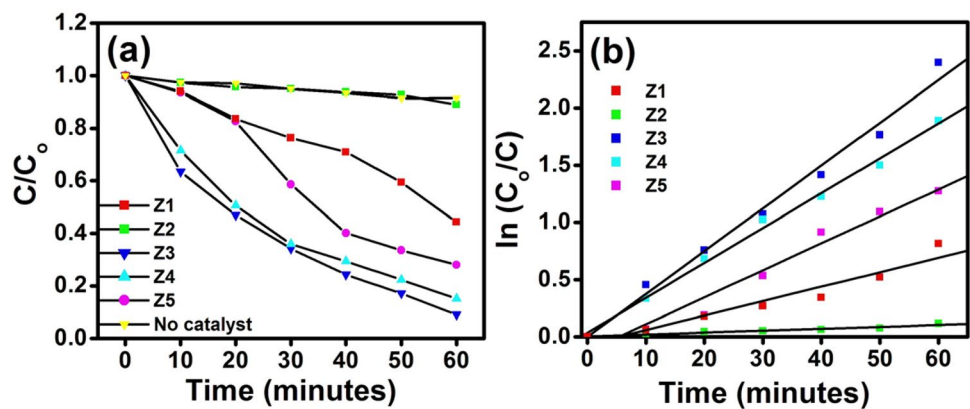

Table 2 Comparison of photodegradation efficiency of the synthesized photocatalysts for *p*-nitrophenol

Sample code	Efficiency (%)	Rate constant (min^{-1})	R
Z1	55.7	0.012	0.96
Z2	11.0	0.002	0.97
Z3	90.9	0.037	0.99
Z4	84.8	0.030	0.99
Z5	72.0	0.024	0.98

mechanism of photocatalysis in ZnO–ZnS heterostructures can be explained on the basis of band structures of the samples (Fig. 9). The type II kind of photocatalytic heterostructure is formed and the formation of ZnS shell has resulted in a red shift in the absorption spectra of ZnO core. This results an effective smaller band gap when compared to core and shell materials. Under light exposure, the valence band (VB) electrons get excited to conduction band (CB) in both ZnO and ZnS. The excited electrons
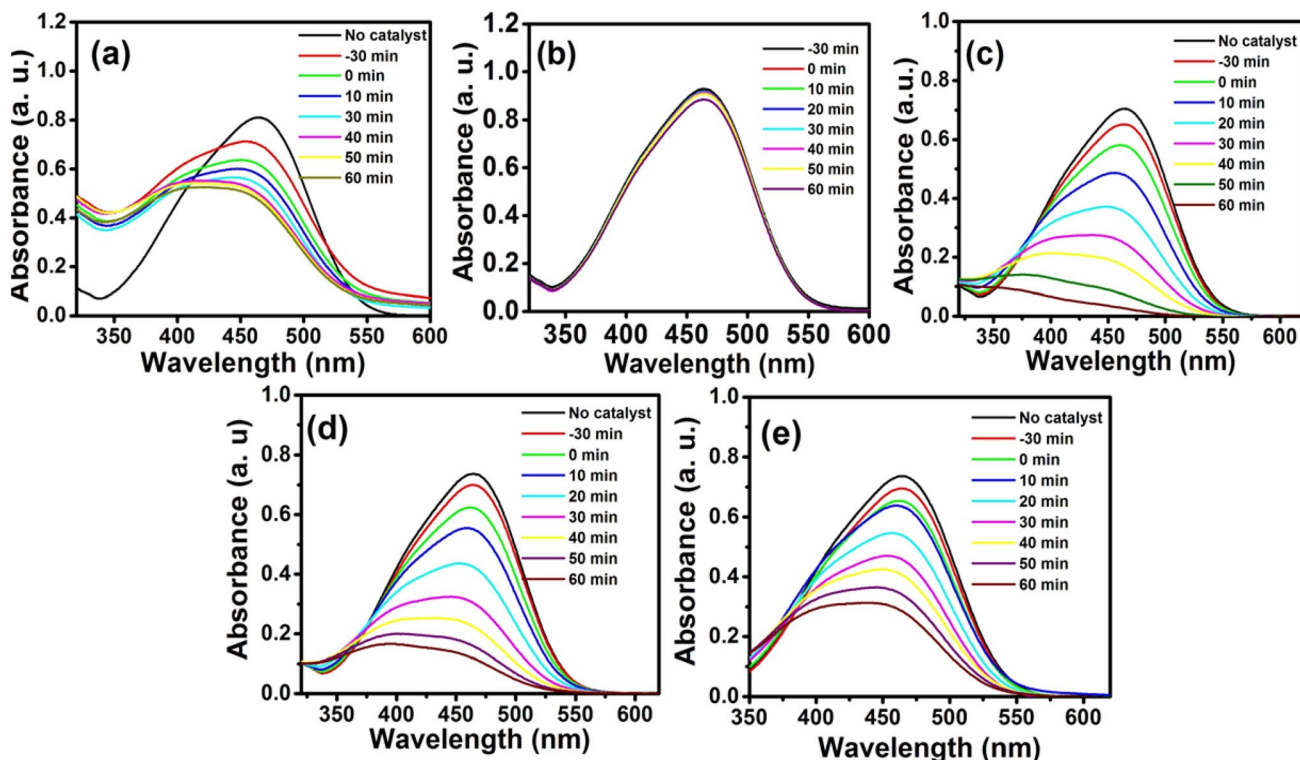
Fig. 7 Photo-degradation study of methyl orange dye under light illumination containing photocatalyst **a** Z1, **b** Z2, **c** Z3, **d** Z4 and **e** Z5
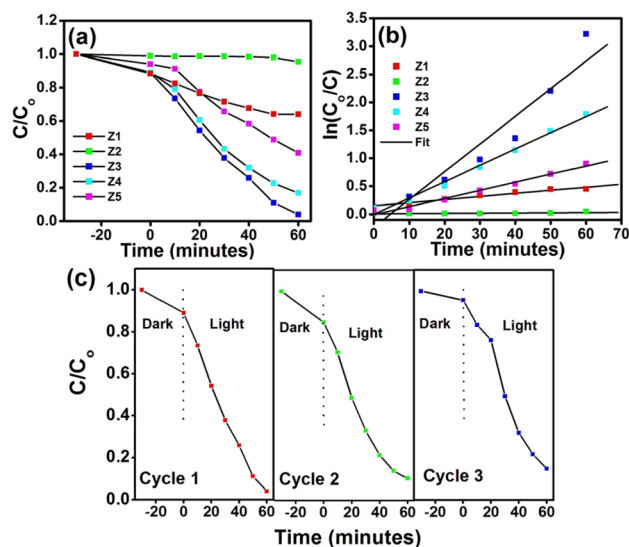

Table 3 Comparison of photodegradation efficiency of the synthesized photocatalysts for methyl orange

| Sample code	Efficiency (%)	Rate constant (min^{-1})	R
Z1	37.1	0.006	0.98
Z2	4.7	0.001	0.98
Z3	96.3	0.049	0.96
Z4	83.4	0.029	0.99
Z5	59.2	0.014	0.99

Fig. 8 a Comparison, **b** kinetics of Photo-degradation of methyl orange under light illumination containing different photocatalyst and **c** recyclability test of Z3 for the degradation of MO up to 3 cycles

move from CB (ZnS) to CB (ZnO) and generated holes from VB (ZnO) to VB (ZnS). This transfer process increases the

separation between the electrons and holes which slowdown the recombination of electron-hole pair in the heterostructure. The reactive oxygen species are generated due to the reaction of photo-generated electron and holes in the semiconductor with surface adsorbed water molecules. The electrons in CB (ZnO) will combine with adsorbed O_2 and produce $^{\bullet}O_2^{-}$ species. The holes accumulated in VB (ZnS) react with adsorbed H_2O molecules and generate OH$^{\bullet}$ species in the solution. These OH$^{\bullet}$ and $^{\bullet}O_2^{-}$ species are very oxidative and reductive respectively and consequently convert the MO molecules into smaller degraded molecules, H_2O and CO_2. The reactions in the process involved are given below [2] -

Table 4 Comparison of ZnO–ZnS core shell heterostructures with literature

S. No.	System and structure	Light source	Photocatalytic efficiency for MO	Photocatalytic efficiency for PNP	Ref
1	ZnO@ZnS hollow dumbbells–graphene composites	Mercury lamp	Efficiency =94% in 40 min Rate constant =0.082 min^{-1},	–	[28]
2	Spherical ZnO/ZnS core/shell particles	UV radiation	Efficiency =95% in 2 h,	–	[31]
3	ZnO/ZnS sheets	Sunlight	Efficiency =~83% in 4 h	–	[38]
4	ZnO/ZnS nanorod array	300 W Hg lamp	Efficiency=~96% in 660 min	–	[40]
5	ZnO@ZnS/C nanofibres	UV (365 nm)	Efficiency =92.2 % in 75 min Rate constant =0.0358 min^{-1}	–	[41]
6	ZnO–ZnS nanowire	UV-light ($\lambda > 324$ nm).	Efficiency= 96% in 40 min Rate constant= 0.072 min^{-1}	–	[57]
7	ZnS-ZnO/Graphene	visible light (400 W)	Efficiency =97.5% for 160 minutes Rate constant =0.011 min^{-1}	Efficiency=96.3% in 140 min	[44]
8	ZnO/ZnS nanosphere	UV light	Efficiency=70% in 2 h	–	[58]
9	Hollow ZnO core/ZnS shell structure	UV lamps	Efficiency=93.7% within 60 min	–	[59]
10	ZnO-ZnS core shell structures	Visible light (>400 nm)	Efficiency =96.3% in 60 min Rate constant=0.049 min^{-1}	Efficiency =90. 9% in 60 min Rate constant =0.037 min^{-1}	This work
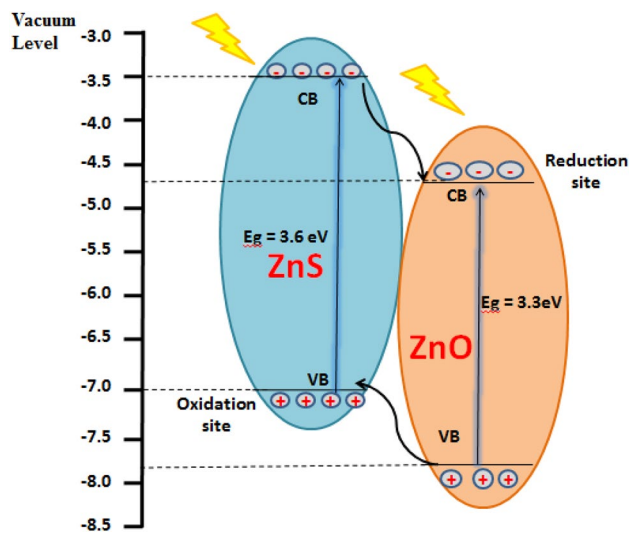
Fig. 9 Schematics for the electron and hole transfer in the ZnO–ZnS heterostructures
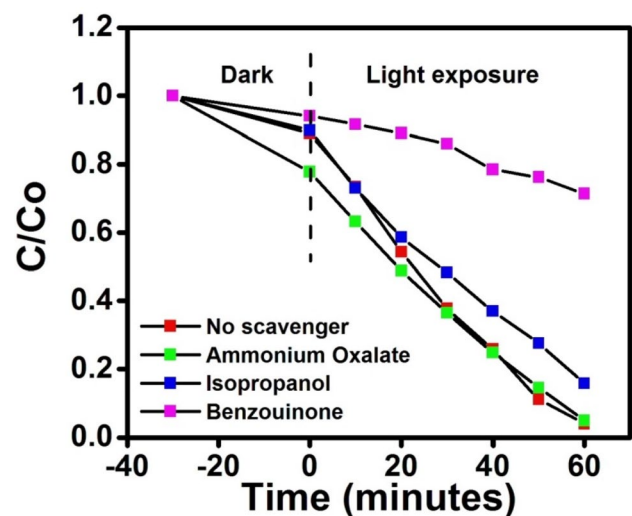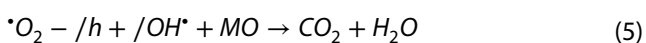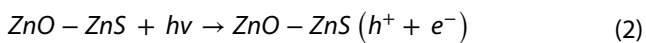
Fig. 10 The scavenger studies for the detection of active species for the photodegradation of methyl orange in the presence of Z3

$$ZnO - ZnS + hv \rightarrow ZnO - ZnS \left(h^+ + e^- \right) \qquad (2)$$

$$H_2O + h^+ \rightarrow OH^\bullet \qquad (3)$$

$$O_2^- + e^- \rightarrow {}^\bullet O_2^- \qquad (4)$$

$${}^\bullet O_2 - /h + /OH^\bullet + MO \rightarrow CO_2 + H_2O \qquad (5)$$

Therefore, the heterostructure shows higher photodegradation efficiency than that of pure ZnO and ZnS [35, 36]. The light illumination over the catalyst will generate electrons (e$^-$) and holes (h$^+$). Further, these photoexcited electrons and holes will combine with surface adsorbed H_2O and O_2 and generate superoxide radical anions (${}^\bullet O_2{}^-$) and hydroxyl radicals (OH$^\bullet$). These *in-situ* generated four active species (e$^-$, h$^+$, OH$^\bullet$ and ${}^\bullet O_2{}^-$) are responsible for the oxidation of organic dye pollutants. For identification of the principal active species during the degradation of MO with ZnO–ZnS as photocatalyst,

different trapping agents were added to reaction solution i.e. ammonium oxalate for holes (h^+), isopropanol for hydroxyl radicals ($OH^•$) and benzoquinone for superoxide radical anions ($^•O_2^-$) before the addition of photocatalyst (Fig. 10). In the absence of any added trapping agent, the photocatalyst degraded MO up to ~ 97.1% in 60 min. When the benzoquinone is added to the dye solution, the maximum quenching was observed (~ 28.7%) in photocatalysis. In case of addition of isopropanol (~ 84.3%) and ammonium oxalate (~ 95.2%), there is not much reduction in photocatalysis rate was observed. From these results, it appears that superoxide radical anions generated in solution are mainly responsible for the degradation of the dyes [52]. Photoluminescence (PL) technique is used for monitoring the recombination of electron hole pair within a semiconductor. It is known that when the rate of recombination of electron-hole is slow down, then, there is a reduction in PL peak intensity. The PL spectra of ZnO–ZnS heterostructures in comparison to bare ZnO excited at a wavelength of 350 nm are shown in Fig. 11. The emission peak for bare ZnO nanorods is obtained at ~ 390 nm. This UV emission arises from the recombination of the free electron-hole pairs via collision of exciton-exciton within the semiconductor [53]. The delay in the recombination of electron and hole due to their separation at the heterojunction of ZnO–ZnS heterostructures result the suppression in the emission signal [54]. PL also shows that Z3 has lowest intensity which indicates that it has slower recombination rate for electron and holes therefore, they can be available for photocatalytic reaction, and hence, it is showing highest catalytic activity. In order to compare the dark and light illuminated behavior of heterostructures with its bare counterparts, transient current response was measured. The typical photocurrent density (J) vs. time plot is shown in Fig. 12a. There was negligible photo-response observed in the bare ZnS whereas photocurrent was degrading with time in case of ZnO due to fast recombination rate of excitons. In the case of ZnO–ZnS heterostructures, there was a significant enhancement in the current on light illumination which again drops gradually after the removal of light source. The EIS studies were carried out to acquire the insights of the enhanced photocatalytic properties in case of Z3 heterostructure. The EIS studies were done in the absence and presence of light. The Nyquist plot of (Fig. 12b) showed a smaller arc radius in the light illumination than dark conditions. This confirmed that there is a low transfer barrier of electron and faster interfacial charge transfer occurs on heterostructure interface, hence, more efficient charge separation happens when
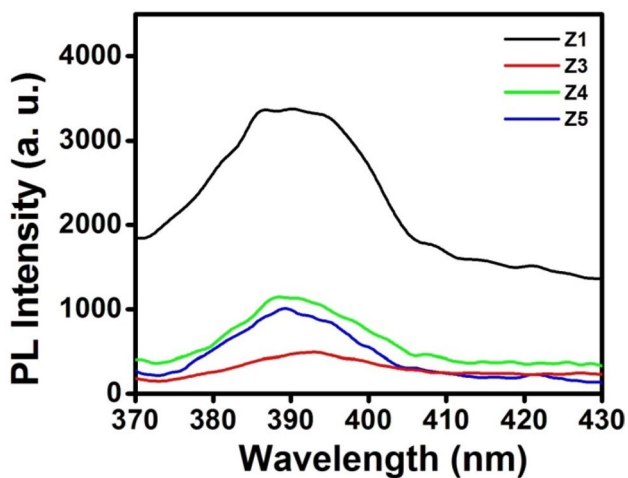

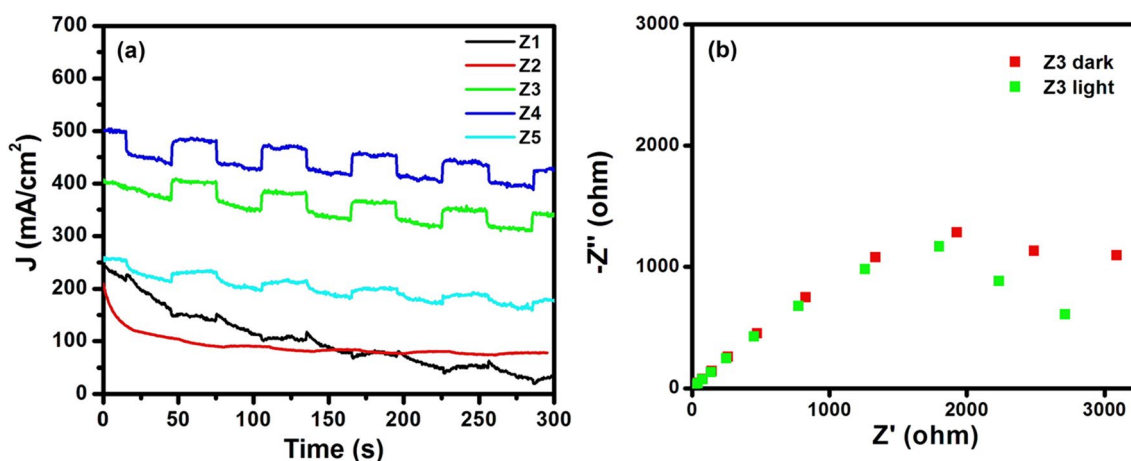**Fig. 11** Photoluminescence studies of ZnO–ZnS heterostructures in comparison to ZnO

Fig. 12 **a** Transient photoresponse of ZnO–ZnS heterostructures and **b** EIS studies for Z3 in presence and absence of light

it is illuminated under light compared to dark conditions. This observation is in closed agreement with earlier reports wherein SnO_2/SnS_2 heterostructure showed higher current density when light is switched on and it drops again when the light is off [55]. The micro-structural characterization of ZnO and its heterostructures have been also done by performing EPR spectroscopy (Fig. S7). This technique is a useful tool to monitor the presence of radical species and the behavior of the present native defects, such as oxygen and/or zinc vacancies. EPR spectra of the bare ZnO showed two signals at $g = 1.9580$ and $g = 2.0036$. The first peak is usually attributed to the shallow donor caused by the surface oxygen vacancies and interstitial Zn atoms. At the same time, the signal at $g = 2.0024$ is attributed to the presence of Zn vacancies. These results evidence the presence of a high concentration of defects in the ZnO nanorods. Also, a sharp decrease in the intensity of peak at $g = 1.9580$ has been observed for the ZnO–ZnS heterostructures with respect to the bare ZnO. This clearly indicates that the relative lower concentration of oxygen vacancies in heterostructures, confirming that Sulphur is occupying the oxygen vacancies [56]. The synthesis of ZnO–ZnS core shell heterostructures with optimized composition can be utilized as an effective photocatalyst for the removal of toxic pollutant from the industrial aqueous waste.

4 Conclusions

ZnO–ZnS heterostructures were successfully synthesized by solid state solvent free route. Sulphurization of ZnO nanorods has been done by utilizing the thiourea as sulphur source. The ratio of ZnO and ZnS can be controlled by varying the amount of sulphur source. Further, the as synthesized ZnO–ZnS heterostructure were utilized for removal of industrial waste (p-nitrophenol and methyl orange) from contaminated water. The Z3 has shown the maximum efficiency for PNP (~ 90%) and MO (~ 97.1%) under the light exposure. It is observed that Z3 consists of optimum amount of ZnO and ZnS in the ZnO–ZnS core–shell heterostructure. The heterostructure formation led to the effective separation of the electron and hole which in result decrease the recombination time, hence, these electrons and holes are available for photocatalytic activity. To confirm this, PL studies of ZnO–ZnS heterostructures has been done. We observed that Z3 shows maximum decrease in the PL intensity in comparison to bare ZnO. The details of photocatalytic activity have been explored by trapping agent studies. Thus, our studies show that ZnO–ZnS are the potential material with non-toxic nature which can work as an efficient photocatalyst for

the waste water treatment to address the environmental pollution issues.

Declarations

References

1. Wang Q, Zhang Z, Liao Q et al (2018) Enhanced field emission properties of graphene-based cathodes fabricated by ultrasonic atomization spray. RSC Adv 8:16207–16213. https://doi.org/10.1039/c8ra02154f
2. Malefane ME, Feleni U, Mafa PJ, Kuvarega AT (2020) Fabrication of direct Z-scheme Co3O4/BiOI for ibuprofen and trimethoprim degradation under visible light irradiation. Appl Surf Sci 514:145940. https://doi.org/10.1016/j.apsusc.2020.145940
3. Li YS, Li TT, Song XF et al (2020) Enhanced adsorption-photocatalytic reduction removal for Cr (VI) based on functionalized TiO_2 with hydrophilic monomers by pre-radiation induced grafting-ring opening method. Appl Surf Sci 514:145789. https://doi.org/10.1016/j.apsusc.2020.145789
4. Bera A, Basak D (2010) Photoluminescence and photoconductivity of ZnS-coated ZnO nanowires. ACS Appl Mater Interfaces 2:408–412. https://doi.org/10.1021/am900686c
5. Bathula B, Koutavarapu R, Shim J, Yoo K (2020) Facile one-pot synthesis of gold/tin oxide quantum dots for visible light catalytic degradation of methylene blue: Optimization of plasmonic effect. J Alloys Compd 812:152081. https://doi.org/10.1016/j.jallcom.2019.152081
6. Li M, Zhu Q, Li J, Kim B (2020) Applied surface science elongation of $ZnWO_4$ nanocrystals for enhanced photocatalysis and the effects of Ag decoration. Appl surface sci 515:146011. https://doi.org/10.1016/j.apsusc.2020.146011
7. Rakibuddin M, Ananthakrishnan R (2017) Fabrication of graphene aerosol hybridized coordination polymer derived CdO/SnO_2 heteronanostructure with improved visible light photocatalytic performance. Sol Energy Mater Sol Cells 162:62–71. https://doi.org/10.1016/j.solmat.2016.12.018
8. Cho S, Jang JW, Lee JS, Lee KH (2012) Porous ZnO-ZnSe nanocomposites for visible light photocatalysis. Nanoscale 4:2066–2071. https://doi.org/10.1039/c2nr11869f
9. Jung HJ, Koutavarapu R, Lee S et al (2018) Enhanced photocatalytic activity of Au-doped Au@ZnO core-shell flower-like nanocomposites. J Alloys Compd 735:2058–2066. https://doi.org/10.1016/j.jallcom.2017.11.378

10. Sadollahkhani A, Kazeminezhad I, Lu J et al (2014) Synthesis, structural characterization and photocatalytic application of ZnO@ZnS core-shell nanoparticles. RSC Adv 4:36940–36950. https://doi.org/10.1039/c4ra05247a

11. Zhang YG, He HY, Pan BC (2013) Tailoring the band gap of ZnO/MgZnO coaxial nanowires by the size and the component of Mg. Phys Chem Chem Phys 15:2932–2936. https://doi.org/10.1039/c2cp44130f

12. Wang G, Li M, Chen C et al (2016) Enhanced field emission properties of ZnO-Ag2S core-shell heterojunction nanowires. Dalt Trans 45:8777–8782. https://doi.org/10.1039/c6dt00711b

13. Zhou Q, Li L, Xin Z et al (2020) Visible light response and heterostructure of composite CdS@ZnS–ZnO to enhance its photocatalytic activity. J Alloys Compd 813:152190. https://doi.org/10.1016/j.jallcom.2019.152190

14. Tie L, Yu C, Zhao Y et al (2018) Fabrication of WO3 nanorods on reduced graphene oxide sheets with augmented visible light photocatalytic activity for efficient mineralization of dye. J Alloys Compd 769:83–91. https://doi.org/10.1016/j.jallcom.2018.07.176

15. Baranowska-Korczyc A, Sobczak K, Dłuzewski P et al (2015) Facile synthesis of core/shell ZnO/ZnS nanofibers by electrospinning and gas-phase sulfidation for biosensor applications. Phys Chem Chem Phys 17:24029–24037. https://doi.org/10.1039/c5cp02278a

16. Hsu YK, Chen YC, Lin YG (2015) Novel ZnO/Fe2O3 core-shell nanowires for photoelectrochemical water splitting. ACS Appl Mater Interfaces 7:14157–14162. https://doi.org/10.1021/acsami.5b03921

17. Zeng F, Huang W-Q, Xiao J-H et al (2018) Isotype heterojunction g-C3N4/g-C3N4 nanosheets as 2D support to highly dispersed 0D metal oxide nanoparticles: Generalized self-assembly and its high photocatalytic activity. J Phys D Appl Phys 52:25501. https://doi.org/10.1088/1361-6463/aae81a

18. Xu J, Sang H, Wang X, Wang K (2015) Facile synthesis and photocatalytic properties of ZnO core/ZnS-CdS solid solution shell nanorods grown vertically on reductive graphene oxide. Dalt Trans 44:9528–9537. https://doi.org/10.1039/c5dt00293a

19. Meng XQ, Peng H, Gai YQ, Li J (2010) Influence of ZnS and MgO shell on the photoluminescence properties of ZnO core/shell nanowires. J Phys Chem C 114:1467–1471. https://doi.org/10.1021/jp909176p

20. Chen CY, Lin CA, Chen MJ et al (2009) ZnO/Al2O3 core-shell nanorod arrays: Growth, structural characterization, and luminescent properties. Nanotechn. 20(18):185605. https://doi.org/10.1088/0957-4484/20/18/185605

21. Khanchandani S, Kundu S, Patra A, Ganguli AK (2013) Band gap tuning of ZnO/In2S3 core/shell nanorod arrays for enhanced visible-light-driven photocatalysis. J Phys Chem C 117:5558–5567. https://doi.org/10.1021/jp310495j

22. Khanchandani S, Kundu S, Patra A, Ganguli AK (2012) Shell thickness dependent photocatalytic properties of ZnO / CdS. J Phys Chem C 116:23653

23. Khanchandani S, Srivastava PK, Kumar S et al (2014) Band gap engineering of ZnO using core/shell morphology with. Inorg Chem 53:8912–8902. https://doi.org/10.1021/ic500518a

24. Subash B, Krishnakumar B, Pandiyan V et al (2012) An efficient nanostructured Ag2S-ZnO for degradation of acid black 1 dye under day light illumination. Sep Purif Technol 96:204–213. https://doi.org/10.1016/j.seppur.2012.06.002

25. Shi XF, Xia XY, Cui GW et al (2015) Multiple exciton generation application of PbS quantum dots in ZnO@PbS/graphene oxide for enhanced photocatalytic activity. Appl Catal B Environ 163:123–128. https://doi.org/10.1016/j.apcatb.2014.07.054

26. Longo E, Flores EM, Raubach CW, Cava S (2016) Optical and structural investigation of ZnO @ ZnS core e shell. Mater chem and phys 173:347–354

27. Liang YC, Lo YR, Wang CC, Xu NC (2018) Shell layer thickness-dependent photocatalytic activity of sputtering synthesized hexagonally structured ZnO-ZnS composite nanorods. Mater (Basel) 11(1):87. https://doi.org/10.3390/ma11010087

28. Yu X, Zhang G, Cao H et al (2012) ZnO@ZnS hollow dumbbells-graphene composites as high-performance photocatalysts and alcohol sensors. New J Chem 36:2593–2598. https://doi.org/10.1039/c2nj40770a

29. Cao G, Yang H, Hong K et al (2015) Synthesis of long ZnO/ZnS core-shell nanowires and their optical properties. Mater Lett 161:278–281. https://doi.org/10.1016/j.matlet.2015.08.127

30. Schrier J, Demchenko DO, Wang LW, Alivisatos AP (2007) Optical properties of ZnO/ZnS and ZnO/ZnTe heterostructures for photovoltaic applications. Nano Lett 7:2377–2382. https://doi.org/10.1021/nl071027k

31. Li W, Song G, Xie F et al (2013) Preparation of spherical ZnO/ZnS core/shell particles and the photocatalytic activity for methyl orange. Mater Lett 96:221–223. https://doi.org/10.1016/j.matlet.2013.01.077

32. Chen W, Ruan H, Hu Y et al (2012) One-step preparation of hollow ZnO core/ZnS shell structures with enhanced photocatalytic properties. CrystEngComm 14:6295–6305. https://doi.org/10.1039/c2ce25591j

33. Chen HM, Chen CK, Liu RS et al (2011) A new approach to solar hydrogen production: A ZnO-ZnS solid solution nanowire array photoanode. Adv Energy Mater 1:742–747. https://doi.org/10.1002/aenm.201100246

34. Liu C, Liu Z, Li J et al (2013) Cu-doping ZnO/ZnS nanorods serve as the photoanode to enhance photocurrent and conversion efficiency. Microelectron Eng 103:12–16. https://doi.org/10.1016/j.mee.2012.09.006

35. Zou Z, Yang X, Zhang P et al (2019) Trace carbon-hybridized ZnS/ZnO hollow nanospheres with multi-enhanced visible-light photocatalytic performance. J Alloys Compd 775:481–489. https://doi.org/10.1016/j.jallcom.2018.10.116

36. Chang YC (2016) Complex ZnO/ZnS nanocable and nanotube arrays with high performance photocatalytic activity. J Alloys Compd 664:538–546. https://doi.org/10.1016/j.jallcom.2016.01.010

37. Yang L, Zhao Z, Wang H et al (2019) Synthesis of ZnO/ZnS core/shell microsphere and its photocatalytic activity for methylene blue and eosin dyes degradation. J Dispers Sci Technol. 41(14):2152–2158. https://doi.org/10.1080/01932691.2019.1653768

38. Yu X, Wei P, Li Y (2019) Enhanced sunlight photocatalytic performance of ZnO/ZnS binary heterostructure sheets. Mater Lett 240:284–286. https://doi.org/10.1016/j.matlet.2018.12.136

39. Ma H, Cheng X, Ma C, et al (2013). Synthesis characterization and hotocatalytic activity of N-Doped ZnO / ZnS composites

40. Liu Z, Lu X, Xie S et al (2011) Facile electrochemical synthesis of ZnO/ZnS heterostructure nanorod arrays. J Electrochem Soc 158:84–87. https://doi.org/10.1149/1.3597611

41. Shami Z, Sharifi-Sanjani N (2014) A well-designed three-dimensional ternary hierarchical co-axial ZnO@ZnS heteroarchitecture decorated electrospun carbon hollow tube nanofibrous mat: Improved ultraviolet-light photocatalytic performance. Cryst Eng Comm 16:910–921. https://doi.org/10.1039/c3ce41513a

42. Sadollahkhani A, Nur O, Willander M et al (2015) A detailed optical investigation of ZnO@ZnS core-shell nanoparticles and their photocatalytic activity at different pH values. Ceram Int 41:7174–7184. https://doi.org/10.1016/j.ceramint.2015.02.040

43. Lin D, Wu H, Zhang R et al (2010) Facile synthesis of heterostructured ZnO-ZnS nanocables and enhanced photocatalytic

activity. J Am Ceram Soc 93:3384–3389. https://doi.org/10.1111/j.1551-2916.2010.03855.x

44. Lonkar SP, Pillai VV, Alhassan SM (2018) Facile and scalable production of heterostructured ZnS-ZnO/Graphene nano-photocatalysts for environmental remediation. Sci Rep 8:1–14. https://doi.org/10.1038/s41598-018-31539-7

45. Sunaina SM, Ghosh S, Mehta SK et al (2017) Investigation of the growth mechanism of the formation of ZnO nanorods by thermal decomposition of zinc acetate and their field. Cryst Eng Comm 19:2264–2270. https://doi.org/10.1039/C7CE00073A

46. Khanchandani S, Kumar S, Ganguli AK (2016) Comparative study of TiO_2/CuS core/shell and composite nanostructures for efficient visible light photocatalysis. ACS Sustain Chem Eng 4:1487–1499. https://doi.org/10.1021/acssuschemeng.5b01460

47. Liu S, Wang X, Zhao W et al (2013) Synthesis, characterization and enhanced photocatalytic performance of Ag_2S-coupled ZnO/ZnS core/shell nanorods. J Alloys Compd 568:84–91. https://doi.org/10.1016/j.jallcom.2013.03.149

48. Liu Y, Gu Y, Yan X et al (2015) Design of sandwich-structured ZnO/ZnS/Au photoanode for enhanced efficiency of photoelectrochemical water splitting. Nano Res 8:2891–2900. https://doi.org/10.1007/s12274-015-0794-y

49. Devi MM, Sunaina SH et al (2019) New approach for the transformation of metallic waste into nanostructured Fe_3O_4 and SnO_2 - Fe_3O_4 heterostructure and their application in treatment of organic pollutant. Waste Manag 87:719–730. https://doi.org/10.1016/j.wasman.2019.03.007

50. Kaur J, Kaur K, Mehta SK, Matharu AS (2020) A novel molybdenum oxide-Starbon catalyst for wastewater remediation. J Mater Chem A 8:14519–14527. https://doi.org/10.1039/d0ta05388k

51. Bhattacharjee A, Ahmaruzzaman M (2015) Photocatalytic-degradation and reduction of organic compounds using SnO_2 quantum dots (via a green route) under direct sunlight. RSC Adv 5:66122–66133. https://doi.org/10.1039/c5ra07578e

52. Singh J, Arora A, Basu S (2019) Synthesis of coral like WO_3/g-C_3N_4 nanocomposites for the removal of hazardous dyes under visible light. J Alloys Compd 808:151734. https://doi.org/10.1016/j.jallcom.2019.151734

53. Saikia L, Bhuyan D, Saikia M et al (2015) Photocatalytic performance of ZnO nanomaterials for self sensitized degradation of malachite green dye under solar light. Appl Catal A Gen 490:42–49. https://doi.org/10.1016/j.apcata.2014.10.053

54. Shaikh AF, Arbuj SS, Tamboli MS et al (2017) ZnSe/ZnO Nanoheterostructures for enhanced solar light hydrogen generation. ChemSelect 2:9174–9180. https://doi.org/10.1002/slct.201701618

55. Sunaina YKK, Ankush et al (2020) Mechanistic insights of enhanced photocatalytic efficiency of SnO2-SnS2 heterostructures derived from partial sulphurization of SnO2. Sep Purif Technol 242:116835. https://doi.org/10.1016/j.seppur.2020.116835

56. Papari GP, Silvestri B, Vitiello G et al (2017) Morphological, structural, and charge transfer properties of F-doped ZnO: a spectroscopic investigation. J Phys Chem C 121:16012–16020. https://doi.org/10.1021/acs.jpcc.7b04821

57. Gao X, Wang J, Yu J, Xu H (2015) Novel ZnO-ZnS nanowire arrays with heterostructures and enhanced photocatalytic properties. CrystEngComm 17:6328–6337. https://doi.org/10.1039/c5ce01078k

58. Wang C, Liu H, Zhou G, Li T (2018) Templated synthesis and Photocatalytic activity of ZnO/ZnS heterojunction. Russ J Phys Chem A 92:200–203

59. Yu L, Chen W, Li D et al (2015) Inhibition of photocorrosion and photoactivity enhancement for ZnO via specific hollow ZnO core/ZnS shell structure. Appl Catal B Environ 164:453–461. https://doi.org/10.1016/j.apcatb.2014.09.055